Specific heat of the ytterbium monopnictides above 5 K from a band-structure calculation

R. Monnier and L. Degiorgi
Laboratorium für Festkörperphysik, Eidgenössische Technische Hochschule, Hönggerberg, CH-8093 Zürich, Switzerland

B. Delley
Paul-Scherrer Institut, RCA Laboratories, CH-8048 Zürich, Switzerland
(Received 31 May 1989; revised manuscript received 29 August 1989)

Applying the self-consistent large-degeneracy expansion to the degenerate Anderson impurity model in the presence of crystal fields, we compute the specific heat of YbN, YbP, and YbAs above 5 K. Each crystal-field level couples to the band states with its own hybridization function, determined from a tight-binding fit to an *ab initio* band-structure calculation. The different amplitudes of the couplings naturally explain the anomalous crystal-field splittings observed by inelastic neutron scattering. Our calculations reproduce the hitherto unexplained excess specific-heat peak seen in all three compounds around 5 K, which we interpret as being due to the Kondo effect for the ground-state doublet.

INTRODUCTION

The occurrence of a broad hump in the specific heat of all ytterbium pnictides around 5 K,[1,2] with no apparent relation to the Schottky anomaly expected from the crystal-field splitting of the $4f^{13}\,^2F_{7/2}$ ground state of the Yb ion measured by inelastic neutron scattering,[3-5] has led to the conjecture that the quasiparticles in these compounds are heavy fermions.[6] As will be shown below, the above feature is a natural consequence of the interplay between crystal field and Kondo effect for an isolated magnetic impurity, and the coherent or Bloch-type nature of the quasiparticle states needs not be invoked. This is also true for the interactions between the rare-earth ions, the scale of which is set by the magnetic ordering temperatures of 0.4 K for YbP (Ref. 7) and 0.6 K for YbAs (Ref. 8) observed by Mössbauer spectroscopy.

Nearly integer-valent rare-earth impurities in metals are commonly described by the infinite-U degenerate Anderson model or the equivalent Coqblin-Schrieffer model, for which the exact ground state[9-12] and thermodynamics[13-15] have been derived in the Bethe ansatz formalism. Recently the method has been generalized to include the presence of crystal fields (CF),[16-18] and explicit curves for the temperature-dependent excess specific heat have been given for different CF configurations.[17,18] For a doublet ground state which is the case of interest in the present context,[3-5] and crystal-field splitting comparable to[18] or larger than[17] the characteristic Kondo temperature T_0 of the unsplit multiplet, the specific heat displays a well-resolved two-peak structure. The peak at low temperature corresponds to the Kondo resonance of the ground-state doublet, with an effective Kondo temperature $T_{\rm eff}$ strongly reduced with respect to T_0.[19] The upper peak is the Schottky anomaly describing the excitations between the now "magnetic" ground-state doublet and higher CF levels.

Although the Bethe ansatz method leads to an exact solution of the impurity problem, the conditions it imposes on the model in order to insure its integrability are fairly restrictive. In particular it assumes that the coupling to the band states is constant in energy and the same for all crystal-fields levels, which is certainly not true in reality. An alternative approach which does not suffer from this restriction is the self-consistent large-N (=degeneracy) expansion[20-22] in the so-called noncrossing approximation[23] (NCA). For vanishing CF and $N=6$, the temperature-dependent specific heat and magnetic susceptibilities obtained by the two methods are in excellent agreement with each other.[20] As the degeneracy is lowered to 4, the large-N expansion puts the Kondo peak in the specific heat at slightly too high a temperature and fails to reproduce the small finite-temperature maximum observed in the Bethe ansatz result for the magnetic susceptibility.[20] No comparison is available for $N=2$, but we expect the self-consistent approach to yield sufficiently accurate results in the temperature range relevant for our study[24] which, to our knowledge, is the first to include CF effects in the calculation of the specific heat within that framework.

THE MODEL

We consider the infinite-U limit of the degenerate Anderson model in the presence of CF:

$$H^{U=\infty}=H_{\rm band}+H_f^{U=\infty}+H_{\rm mix}^{U=\infty}\ , \tag{1}$$

where $H_{\rm band}$ is obtained from a tight-binding fit to an *ab initio* band-structure calculation, as described in detail in Ref. 25;

$$H_f^{U=\infty}=\varepsilon_{\Gamma_6}\sum_{j=1}^{N_{\Gamma_6}}\hat{n}_{\Gamma_6}^j+\varepsilon_{\Gamma_8}\sum_{j=1}^{N_{\Gamma_8}}\hat{n}_{\Gamma_8}^j+\varepsilon_{\Gamma_7}\sum_{j=1}^{N_{\Gamma_7}}\hat{n}_{\Gamma_7}^j\ , \tag{2}$$

with the bare[26] CF levels ε_{Γ_6} (ground state, degeneracy $N_{\Gamma_6}=2$), ε_{Γ_8} (first excited state, $N_{\Gamma_8}=4$) and ε_{Γ_7} ($N_{\Gamma_7}=2$) for the $4f^{13}F_{7/2}$ multiplet. The $\hat{n}_{\Gamma_i}^j$ are

projection operators on the CF states:

$$\hat{n}^{l}_{\Gamma_i} = |\Gamma_i;j\rangle\langle\Gamma_i;j| \ , \tag{2a}$$

and similarly we define the projector on the full-shell (zero-hole) configuration:

$$\hat{n}_0 = |0\rangle\langle 0| \ . \tag{2b}$$

The mixing matrix elements between localized and band states take a particularly simple form in a tight-binding basis. Numbering the basis vectors by $|\mathbf{k};\alpha\rangle$, we get

$$H^{U=\infty}_{\text{mix}} = \sum_{\substack{\mathbf{k},\nu,\alpha \\ \Gamma_i,j}} [a^{*\nu}_{\alpha}(\mathbf{k}) V^{\Gamma_i,j}_{\mathbf{k},\alpha} c^{\dagger}_{\mathbf{k}\alpha} F_{\Gamma_i,j} + \text{H.c.}] \ , \tag{3}$$

where the normalized eigenvector for band ν at the point $\mathbf{k}$ is given by

$$|\mathbf{k},\nu\rangle = \sum_{\alpha} a^{\nu}_{\alpha}(\mathbf{k})|\mathbf{k};\alpha\rangle \ , \tag{3a}$$

and the operator $c^{\dagger}_{k,\alpha}$ creates a hole in the basis state $|\mathbf{k};\alpha\rangle$;

$$F_{\Gamma_i,j} = |0\rangle\langle\Gamma_i;j| \tag{3b}$$

and

$$V^{\Gamma_i,j}_{\mathbf{k},\alpha} = \langle\mathbf{k};\alpha|V|\Gamma_i;j\rangle \ . \tag{3c}$$

Explicit expression for the matrix elements have been given in Ref. 25 for the semirelativistic case in which only the orbital angular momentum of the f hole is considered. The inclusion of spin-orbit coupling is straightforward and the derivation can be found in Appendix A.

The NCA leads to the following set of coupled integral equations for the empty and occupied state propagators:[20–23]

$$G_0(z) = \left[z - \sum_{\Gamma_i} N_{\Gamma_i} \int \left| V_{\Gamma_i}(\varepsilon) \right|^2 \times G_{\Gamma_i}(z+\varepsilon) f(\varepsilon) d\varepsilon \right]^{-1} , \tag{4a}$$

$$G_{\Gamma_i}(z) = \left[z - \varepsilon_{\Gamma_i} - \int \left| V_{\Gamma_i}(\varepsilon) \right|^2 \times G_0(z-\varepsilon)[1-f(\varepsilon)] d\varepsilon \right]^{-1} , \tag{4b}$$

where $f(\varepsilon)$ is the Fermi distribution function and

$$\left| V_{\Gamma_i}(\varepsilon) \right|^2 = \sum_{\substack{\mathbf{k},\nu \\ \alpha,\beta}} a^{*\nu}_{\alpha}(\mathbf{k}) a^{\nu}_{\beta}(\mathbf{k}) V^{\Gamma_i,j}_{\mathbf{k},\alpha} V^{\Gamma_i,j'*}_{\mathbf{k},\beta} \delta(\varepsilon - \varepsilon^{\nu}_{\mathbf{k}}) \tag{4c}$$

is diagonal in j,j' and describes the hopping of a hole from the level $|\Gamma_i,j\rangle$ to any of the conduction bands and back. In Fig. 1, we show this function for the three CF levels of the f hole in YbN, YbP, and YbAs.

Although all properties can, in principle, be derived from the spectral functions

$$B(\varepsilon) = -\frac{1}{\pi} \text{Im} G_0(\varepsilon + i o^{+}) \ , \tag{5a}$$

$$A_{\Gamma_i}(\varepsilon) = -\frac{1}{\pi} \text{Im} G_{\Gamma_i}(\varepsilon + i 0^{+}) \ , \tag{5b}$$

the fact that they vanish exponentially fast below the NCA ground-state energy E_0 makes it necessary, for numerical reasons, to introduce "negative-frequency-distribution functions"[20,27]

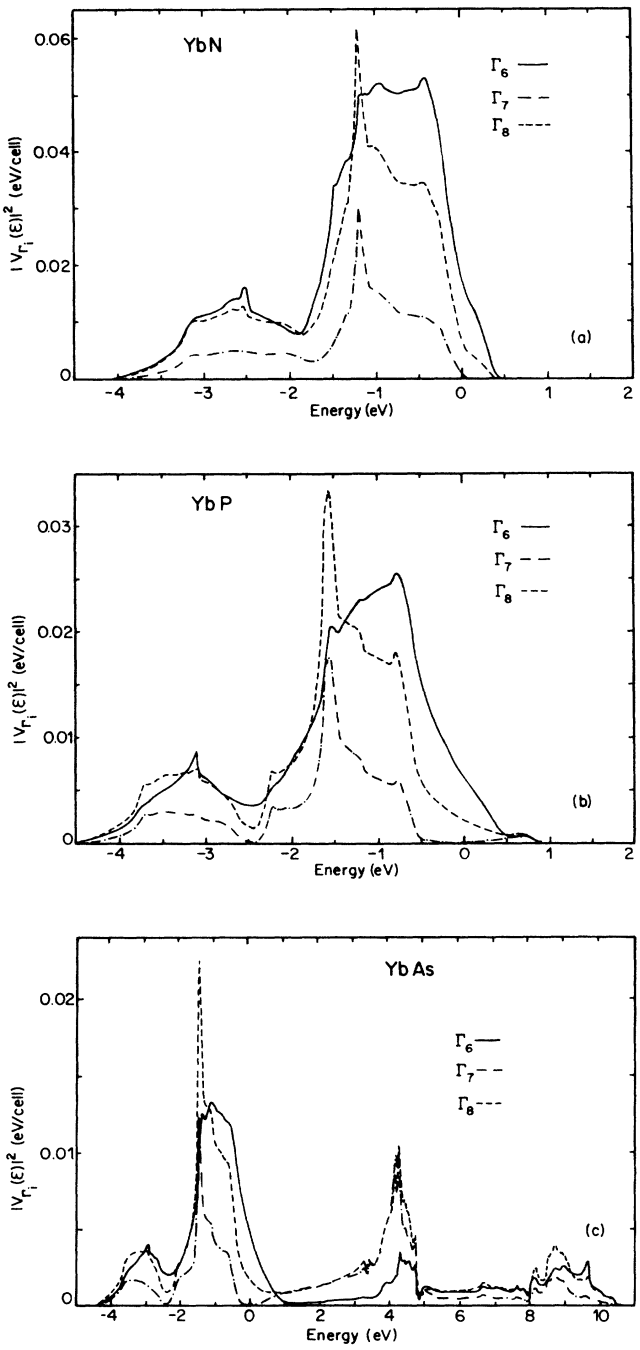

FIG. 1. Energy-dependent coupling functions $|V_{\Gamma_i}(\varepsilon)|^2$, for the three crystal-field levels Γ_6, Γ_8, and Γ_7 of a $4f$ hole on the ytterbium ion in YbN, YbP, and YbAs. The zero of energy is at the Fermi level, which is fixed by imposing charge neutrality. In the first two compounds, the coupling is only to the anion p bands, in YbAs there is a metal-metal d-f hybridization as well.

$$b(\varepsilon)=\frac{1}{Z_f}e^{-\beta(\varepsilon-\varepsilon_0)}B(\varepsilon)\ , \tag{6a}$$

$$a_{\Gamma_i}(\varepsilon)=\frac{1}{Z_f}e^{-\beta(\varepsilon-\varepsilon_0)}A_{\Gamma_i}(\varepsilon)\ , \tag{6b}$$

where Z_f is the impurity partition function

$$Z_f=\int_{-\infty}^{\infty}d\varepsilon\, e^{-\beta\varepsilon}\left[B(\varepsilon)+\sum_{\Gamma_i}N_{\Gamma_i}A_{\Gamma_i}(\varepsilon)\right] \tag{7}$$

and ε_0 is an offset energy chosen for convenience. The function $b(\varepsilon)$ and $a_{\Gamma_i}(\varepsilon)$ must be computed independently as self-consistent solutions of the following new set of coupled integral equations:

$$b(\varepsilon)=|G_0(\varepsilon-i0^+)|^2\times\sum_{\Gamma_i}N_{\Gamma_i}\int\left|V_{\Gamma_i}(\varepsilon')\right|^2 a_{\Gamma_i}(\varepsilon'+\varepsilon)\times[1-f(\varepsilon')]d\varepsilon'\ , \tag{8a}$$

$$a_{\Gamma_i}(\varepsilon)=|G_{\Gamma_i}(\varepsilon-i0^+)|^2\times\int\left|V_{\Gamma_i}(\varepsilon')\right|^2 b(\varepsilon'-\varepsilon)f(\varepsilon')d\varepsilon'\ . \tag{8b}$$

The impurity partition function is then readily obtained as[27]

$$Z_f=B(\varepsilon_0)/b(\varepsilon_0)=A_{\Gamma_i}(\varepsilon_0)/a_{\Gamma_i}(\varepsilon_0),\quad\forall\Gamma_i\ , \tag{9}$$

and from it we derive the excess specific heat in the computationally convenient form:[20]

$$C_{\rm imp}(T)=\left[\frac{\partial^2}{\partial(\ln\beta)^2}-\frac{\partial}{\partial\ln\beta}\right]\ln Z_f(T)\ . \tag{10}$$

From the above defined spectral functions ($\varepsilon_0=0$), we can derive the photoemission and inverse photoemission spectra

$$\rho^{<}(\omega)\equiv\rho_f(\omega)f(\omega)=\sum_{\Gamma_i}N_{\Gamma_i}\int a_{\Gamma_i}(\omega+\varepsilon)B(\varepsilon)d\varepsilon\ , \tag{11a}$$

$$\rho^{>}(\omega)\equiv\rho_f(\omega)[1-f(\omega)]=\sum_{\Gamma_i}N_{\Gamma_i}\int A_{\Gamma_i}(\omega+\varepsilon)b(\varepsilon)d\varepsilon\ , \tag{11b}$$

where the temperature-dependent f density of states

$$\rho_f(\omega)=\rho^{<}(\omega)+\rho^{>}(\omega) \tag{11c}$$

carries all the information concerning the effect of hybridization on the CF splittings.[26]

Finally we introduce the partial f moment spectrum:[20]

$$\sigma_{\Gamma_i}(\omega)\equiv\frac{1}{\pi}\mathrm{Im}\chi_{\Gamma_i}(\omega+i0^+)=\int a_{\Gamma_i}(\varepsilon)[A_{\Gamma_i}(\varepsilon+\omega)-A_{\Gamma_i}(\varepsilon-\omega)]d\varepsilon\ , \tag{12}$$

in terms of which the static spin susceptibility is obtained as a sum of principal value integrals

$$\chi(T)=\frac{1}{3}\sum_{\Gamma_i}N_{\Gamma_i}\mu_{\Gamma_i}^2\,\mathrm{P}\int_{-\infty}^{\infty}\frac{\sigma_{\Gamma_i}(\omega)}{\omega}d\omega\ , \tag{13}$$

where μ_{Γ_i} is the effective high-temperature moment for the level Γ_i [$\sqrt{J(J+1)}g_j\mu_B$ for the unsplit multiplet with total angular momentum J and Landé factor g_j]:

$$\mu_{\Gamma_6}=\sqrt{\tfrac{16}{3}}\mu_B,\quad\mu_{\Gamma_8}=\sqrt{\tfrac{1040}{147}}\mu_B,\quad\mu_{\Gamma_7}=\sqrt{\tfrac{432}{49}}\mu_B\ ,$$

for the $4f^{13}\,{}^2F_{7/2}$ state with $g_{7/2}=\frac{8}{7}$, in a cubic CF.

APPLICATION TO THE YTTERBIUM PNICTIDES

Our approach differs from previous model calculations in that the absolute position of the Fermi level E_F is unambiguously fixed by the condition of charge neutrality for any given f-level occupation n_f. Since the latter is in turn determined by the distance between the manifold of CF levels and E_F, both quantities have to be computed self-consistently. In Table I, we present the parameters used in our calculations. The values of n_f for YbN and YbP are about 5% lower than those obtained from a careful analysis of the $3d$ core-level spectra of the three pnictides[29] with the variational method.[30] Due to the proximity of E_F to the bottom of the (hole) band (see Fig. 1), higher values of the f-level occupation lead to numerical instabilities for these compounds. The CF splittings are taken from inelastic neutron scattering experiments and, in view of the prohibitive computational effort involved, no attempt has been made to extract the position of the bare levels[26] from these measurements. Finally we note that the low hybridization strength of the Γ_7 level allows us to treat it as isolated, which limits its contribution to the specific heat to the region of the Schottky anomaly. Furthermore, due to its high energy, the corresponding component of the static spin susceptibility, Eq. (13), is negligibly small below room temperature.

TABLE I. Parameters used in the calculation of the thermodynamic properties of the ytterbium pnictides. The values of n_f are from the analysis of the $3d$ core-level spectra in Ref. 28. The crystal-field splittings are taken from inelastic neutron scattering experiments. E_0 is the resulting NCA ground-state energy. $E^+(E^-)$ is the peak position of the positive (negative) energy resonance in the $4f$ density of states at 14.6 K.

	YbN	YbP	YbAs
n_f ($T=0$)	0.94	0.95	0.921
$(\varepsilon_{\Gamma_6}-E_F)$ (meV)	−500	−200	−100
$(\varepsilon_{\Gamma_8}-\varepsilon_{\Gamma_6})$ (meV)	55[a]	20[b]	18[c]
$(\varepsilon_{\Gamma_7}-\varepsilon_{\Gamma_6})$ (meV)		32[b]	40[c]
E_0 (meV)	−566.3	−238.8	−128.8
E^+ (meV)	73	34	28
$\lvert E^-\rvert$ (meV)	71	33	25

[a]Ref. 5: The Γ_7 level is not seen, as it is not accessible from the ground state and the Γ_8 level lies too high in energy to be appreciably populated at room temperature.
[b]Ref. 3.
[c]Ref. 4.

In Fig. 2, we present our calculated specific heats and spin susceptibilities[31] for the Γ_6-doublet-Γ_8-quartet configuration on a logarithmic temperature scale. For all three compounds we observe the characteristic two-peak structure in $C_{imp}(T)$ already found in the Bethe Ansatz model calculations.[17,18] Also shown for YbP and YbAs are the Schottky anomalies corresponding to the CF splittings of Table I, with and without inclusion of the Γ_7 level. For YbN, the two-level Schottky anomaly is indistinguishable from our calculated high-temperature peak. A comparison of our low-temperature results with those obtained by Rajan[13] for an isolated doublet shows that the scaling temperature for the specific heat is much

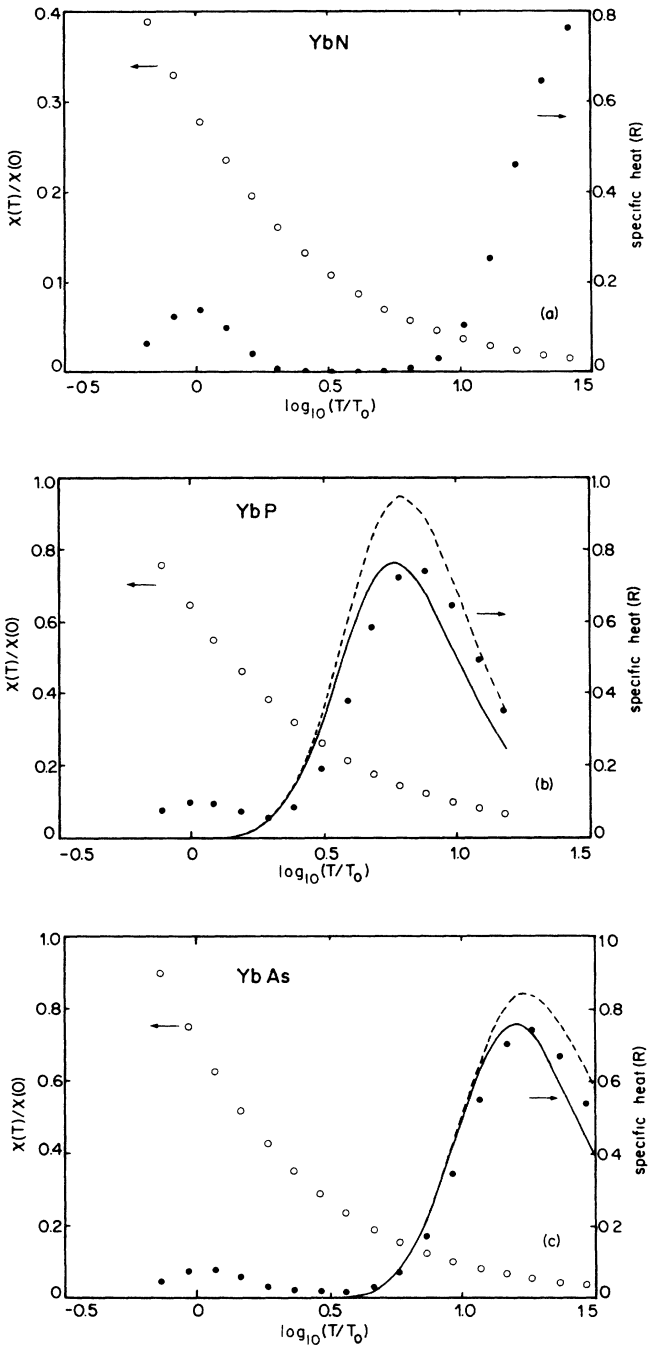

FIG. 2. Specific heat per mole and spin susceptibility normalized to its zero temperature value for (a) YbN, (b) YbP, and (c) YbAs, as obtained from the self-consistent large degeneracy expansion for the crystal-field configuration Γ_6-Γ_8. The temperature is scaled to its value at the first maximum in c_{imp} ($\approx$9, 15, and 5 K, respectively). Also shown for YbP and YbAs are the Schottky anomalies expected for the Γ_6-Γ_8 and Γ_6-Γ_8-Γ_7 crystal-field configurations. For YbN the two-level Schottky anomaly is indistinguishable from the self-consistent result above 20 K.

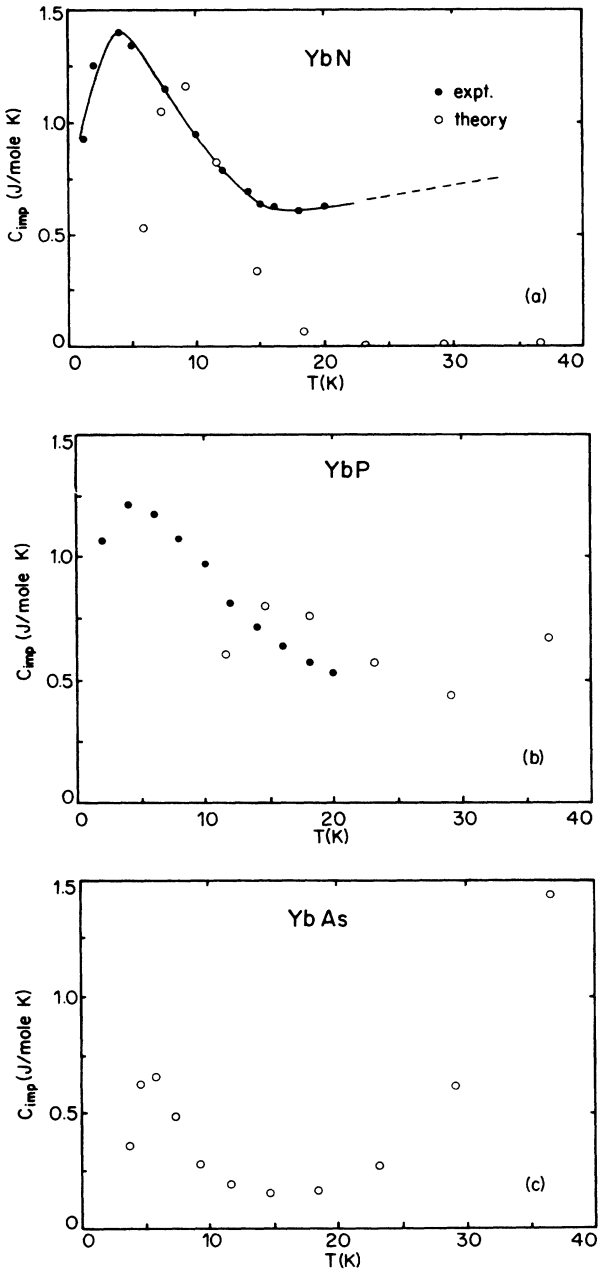

FIG. 3. Calculated specific heats at low temperature (open circles) for (a) YbN, (b) YbP, and (c) YbAs, compared to the experimental ones (solid circles) where available. The latter were obtained by subtracting from the measured values those for the corresponding Lutetium compound: (Ref. 1 for YbN, Ref. 2 for YbP) so as to keep only the contribution due to the open 4*f* shell.

larger than the one for the susceptibility, reflecting the limitations of the self-consistent approach for $N=2$. Nevertheless, as seen in Fig. 3, where $C_{\rm imp}(T)$ is compared with the published experimental data below 40 K, the impurity model does, at least semiquantitatively, account for the observed behavior, and that without adjustable parameters. The origin of the excess specific heat measured in YbN (Ref. 1) above 15 K is not clear. We note, however, that the Schottky anomaly in that experiment has its maximum at ~ 190 K instead of ~ 240 K as expected from the CF splitting, which indicates that the sample may contain other phases. Setting the CF splitting to zero produces the expected *single* peak in $C_{\rm imp}(T)$, of amplitude roughly equal to the one found at high temperature for the configuration with two split levels. In YbAs, our best converged case, the maximum lies at ~ 29 K, which corresponds to a Kondo temperature of ~ 90 K for the unsplit sextuplet.[20]

The $4f$ density of states for a two-level system has been calculated before by Bickers *et al.*[20] in the limit where the singlet binding energy is much smaller than the level splitting Δ (due in their case to the spin-orbit interaction), and the spectrum at positive energies consisted in two narrow peaks separated by Δ. As seen in Table I, the situation here is completely different, the CF splitting being between 20 and 50 percent smaller than the energy $\delta=|E_0-\varepsilon_{\Gamma_6}|$ gained through hybridization with the conduction bands. The positive-energy spectrum consists of a large peak with its maximum near δ, the weight of which is entirely concentrated in the excited level (Γ_8) component. At negative energies one finds the expected broad ionization peak at $\sim\varepsilon_{\Gamma_6}$ and a resonance at roughly δ, which we interpret as being due to the emission of a Fermi-level hole with a simultaneous excitation from the singlet ground state to the relaxed ($\equiv$fully hybridized) excited level Γ_8. In this picture the position of the resonance is a direct measure of the renormalized[26] CF splitting one would observe in an inelastic neutron scattering experiment. As seen in Fig. 4 which shows the $4f$ density of states for YbAs, representative for all three compounds, the spectrum at low temperature also displays the expected Kondo resonance for the ground-state doublet. The corresponding Kondo temperature $T_{\rm eff}$ of ≈ 2.8 K compares well with the position of the maximum in $C_{\rm imp}(T)$ found at ≈ 5 K. On the other hand, the ratio $\sigma_{\Gamma_6}(\omega)/\omega$, which determines the low-temperature susceptibility, clearly reflects the $|\omega|^{-[1/2(N+1)]}$ divergence predicted for the large degeneracy expansion at $T=0$.[27,32] The physical maximum expected at $\approx\pm 1.4 k_B T_{\rm eff}$ is barely discernable as a slight flattening in the wing of a huge peak centered at the origin. As a result, $\chi(T)$ becomes too large and furthermore does not appear to change its curvature.

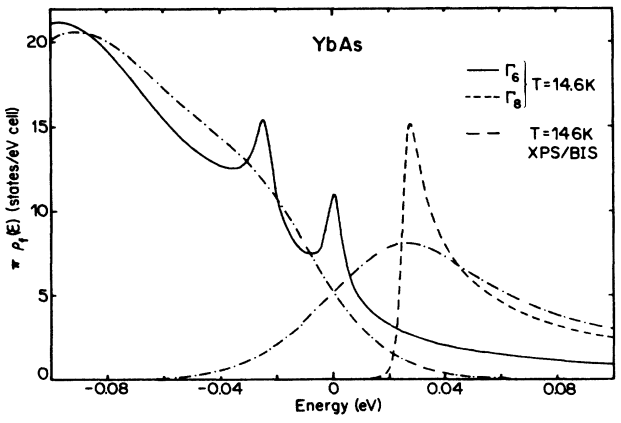

FIG. 4. Temperature-dependent $4f$ density of states in YbAs. At $T=14.6$ K, we show separately the contribution from the Γ_6 ground level and from the excited level Γ_8, weighted by their respective degeneracies. At $T=146$ K, we show the photoemission (XPS) and inverse photoemission (BIS) spectrum.

SUMMARY AND CONCLUSION

We have presented a calculation of the specific heat of the ytterbium pnictides above 5 K, based on the degenerate Anderson impurity model in the presence of crystal fields. Using the hybridization matrix elements obtained from a tight-binding fit to a semirelativistic band-structure calculation, the mixing term in the Anderson Hamiltonian was transformed into an effective, energy-dependent potential for each of the three CF levels Γ_6, Γ_8, and Γ_7 of the $4f$ hole on the Yb ion. The different amplitudes of the three potentials naturally explain the anomalously large CF splittings observed in these compounds by inelastic neutron scattering. Applying the self-consistent large degeneracy expansion to the model with the above potentials leads to a two-peak structure in the specific heat, characteristic of a situation with finite CF splittings. The upper peak is very close to the Schottky anomaly for the corresponding CF configuration, while the one at low temperature is interpreted as being due to the Kondo effect for the Γ_6 ground-state doublet.

Our results strongly suggest that the broad hump seen in the specific heat of all Yb pnictides around 5K is a single-site effect. Also, the logarithmic temperature dependence above $T_{\rm eff}$ predicted by the impurity model is consistent with the very slow approach to $R\ln_2$ observed experimentally.[2,6]

In contrast to the specific heat which is obtained as a thermodynamic derivative, the spin susceptibility by its definition directly reflects the limitations of the self-consistent approach at low temperature and cannot be used to draw any conclusions about the true ground state of the system. We note, however, that the Bethe ansatz treatments do produce a susceptibility whose shape is compatible with the observed one, and that the work of Okiji and Kawakami[33] on the magnetic properties of the Coqblin-Schrieffer model in the presence of crystal fields immediately explains the observation that the magnetization per Yb ion in YbP at 1.6 K and 70 kOe only reaches a third of the saturation value of 1.33 μ_B for the Γ_6 level, as due to the fact that the corresponding Zeeman energy of 0.4 meV is much smaller than the Kondo energy $k_B T_0$ for the unsplit multiplet.

ACKNOWLEDGMENTS

It is a great pleasure to thank D. D. Koelling for providing us with the band structures of the Yb pnictides and for his expert advice on the tight-binding fits. We are grateful to A. Furrer for letting us use his unpublished inelastic neutron scattering data on YbN and YbAs. Finally we thank the Centre de Calcul de l'Ecole Polytechnique Fédérale de Lausanne (EPFL) for the generous allotment of Cray 2 computer time.

APPENDIX A

In a cubic CF the $J=\frac{7}{2}$ ground-state multiplet of the $4f$ hole splits into two doublets and a quartet:

$$|\Gamma_6;1\rangle=\sqrt{\tfrac{5}{12}}|+\tfrac{7}{2}\rangle+\sqrt{\tfrac{7}{12}}|-\tfrac{1}{2}\rangle\ ,$$
$$|\Gamma_6;2\rangle=\sqrt{\tfrac{5}{12}}|-\tfrac{7}{2}\rangle+\sqrt{\tfrac{7}{12}}|+\tfrac{1}{2}\rangle\ , \tag{A1}$$

$$|\Gamma_7;1\rangle=\sqrt{\tfrac{9}{12}}|+\tfrac{5}{2}\rangle-\sqrt{\tfrac{3}{12}}|-\tfrac{3}{2}\rangle\ ,$$
$$|\Gamma_7;2\rangle=\sqrt{\tfrac{9}{12}}|-\tfrac{5}{2}\rangle-\sqrt{\tfrac{3}{12}}|+\tfrac{3}{2}\rangle\ , \tag{A2}$$

$$|\Gamma_8;1\rangle=\sqrt{\tfrac{7}{12}}|\tfrac{7}{2}\rangle-\sqrt{\tfrac{5}{12}}|-\tfrac{1}{2}\rangle\ ,$$
$$|\Gamma_8;2\rangle=\sqrt{\tfrac{7}{12}}|-\tfrac{7}{2}\rangle-\sqrt{\tfrac{5}{12}}|+\tfrac{1}{2}\rangle\ ,$$
$$|\Gamma_8;3\rangle=\sqrt{\tfrac{3}{12}}|+\tfrac{5}{2}\rangle+\sqrt{\tfrac{9}{12}}|-\tfrac{3}{2}\rangle\ , \tag{A3}$$
$$|\Gamma_8;4\rangle=\sqrt{\tfrac{3}{12}}|-\tfrac{5}{2}\rangle+\sqrt{\tfrac{9}{12}}|+\tfrac{3}{2}\rangle\ ,$$

where the kets on the right-hand side are indexed by the z component of the angular momentum. The hybridization matrix elements are independent of spin and couple only to the orbital part of the impurity wave function, for which the CF decomposition is

$$|\Gamma_{2'}\rangle=-\frac{i}{\sqrt{2}}(|2\rangle-|-2\rangle)\ , \tag{A4}$$

$$|\Gamma_{15};x\rangle=\sqrt{\tfrac{3}{16}}(|1\rangle-|-1\rangle)-\sqrt{\tfrac{5}{16}}(|3\rangle-|-3\rangle)\ ,$$
$$|\Gamma_{15};y\rangle=-i\sqrt{\tfrac{3}{16}}(|1\rangle+|-1\rangle)-i\sqrt{\tfrac{5}{16}}(|3\rangle+|-3\rangle)\ , \tag{A5}$$
$$|\Gamma_{15};z\rangle=|0\rangle\ ,$$

$$|\Gamma_{25};y\rangle=-i\sqrt{\tfrac{5}{16}}(|1\rangle+|-1\rangle)+i\sqrt{\tfrac{3}{16}}(|3\rangle+|-3\rangle)\ ,$$
$$|\Gamma_{25};z\rangle=\frac{1}{\sqrt{2}}(|2\rangle+|-2\rangle)\ , \tag{A6}$$
$$|\Gamma_{25};x\rangle=\sqrt{\tfrac{5}{16}}(|1\rangle-|-1\rangle)+\sqrt{\tfrac{3}{16}}(|3\rangle-|-3\rangle)\ ,$$

with the same notation as above, but with m_J replaced by m_L. All states in (A4)–(A6) are doubly degenerate in spin $|+\rangle$ and $|-\rangle$, and the two sets of states (A1)–(A3) and (A4)–(A6) can be related with help of the following relation from elementary quantum mechanics:

$$|J=L+\tfrac{1}{2};m_J\rangle=\left[\frac{J+m_J}{2J}\right]^{1/2}|L;m_J-\tfrac{1}{2}\rangle|+\rangle + \left[\frac{J-m_J}{2J}\right]^{1/2}|L;m_J+\tfrac{1}{2}\rangle|-\rangle\ . \tag{A7}$$

In the semirelativistic treatment of Ref. 25, it was found that the hybridization is dominated by nearest-neighbor ligand-metal $(pf\sigma)$ and $(pf\pi)$ interactions, which led to the following form for the matrix elements (3c):

$$V^{\Gamma_{15},x}_{\mathbf{k},p_x}=N^{-1/2}\left[2(pf\sigma)\cos k_x\frac{a}{2} -(\tfrac{3}{2})^{1/2}(pf\pi)\left[\cos k_y\frac{a}{2}+\cos k_z\frac{a}{2}\right]\right]\ , \tag{A8}$$

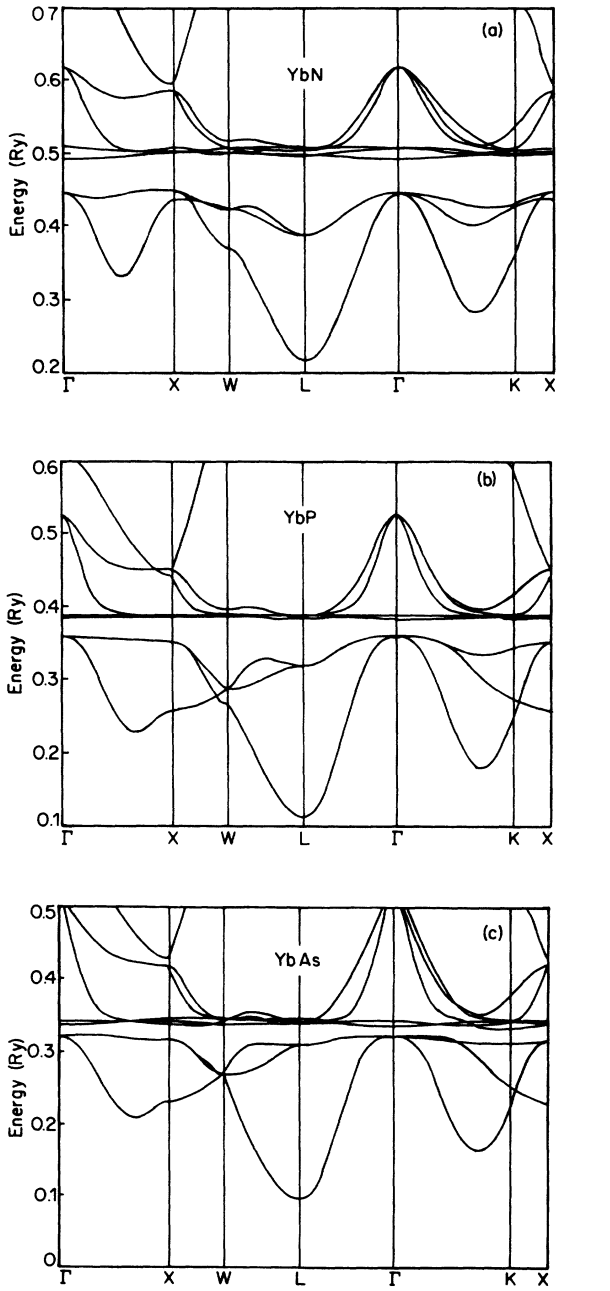

FIG. 5. Self-consistent semirelativistic band structures of YbN, YbP, and YbAs.

$$V_{\mathbf{k},p_x}^{\Gamma_{25},x}=N^{-1/2}(\tfrac{5}{2})^{1/2}(pf\pi)\left[\cos k_y\frac{a}{2}-\cos k_z\frac{a}{2}\right], \quad \text{(A9)}$$

and the corresponding permutation for y and z.

Whereas in YbN and YbP these are the only couplings that need to be considered, in the "more metallic" YbAs it is important to include the *second* -neighbor metal-metal ($df\sigma$) interaction between the Γ_{15}-like f orbitals and the bands derived from the Yb-5d orbitals of e_g symmetry, for which a typical example is

$$V_{\mathbf{k},(3z^2-r^2)}^{\Gamma_{15},z}=N^{-1/2}2i(df\sigma)\sin k_z a \ . \quad \text{(A10)}$$

In (A8)–(A10), N is the number of unit cells in the crystal and a is the lattice constant. If interactions beyond nearest-neighbor metal ligand and second-neighbor metal metal are ignored, the $\Gamma_{2'}$ level does not couple to the bands at all.

After forming the combination (4c) of the above matrix elements, one is left with the following energy-dependent CF Hamiltonian for the impurity in the absence of spin-orbit coupling:

$$H_{\mathrm{SR}}^{\mathrm{CF}}(\varepsilon)=|V_{\Gamma_{15}}(\varepsilon)|^2\sum_{\alpha}|\Gamma_{15};\alpha\rangle\langle\Gamma_{15};\alpha| + |V_{\Gamma_{25}}(\varepsilon)|^2\sum_{\alpha}|\Gamma_{25};\alpha\rangle\langle\Gamma_{25};\alpha| \ . \quad \text{(A11)}$$

After multiplication by the unit operator in spin space, matrix elements can be taken between the states (A1)–(A3) with the result

$$\langle\Gamma_i;j|H_{\mathrm{SR}}^{\mathrm{CF}}(\varepsilon)\otimes\mathbb{1}_{\mathrm{spin}}|\Gamma_{i'};j'\rangle=|V_{\Gamma_i}(\varepsilon)|^2\delta_{\Gamma_i\Gamma_{i'}}\delta_{jj'} \ , \quad \text{(A12)}$$

and

$$|V_{\Gamma_6}(\varepsilon)|^2=|V_{\Gamma_{15}}(\varepsilon)|^2 \ ,$$
$$|V_{\Gamma_8}(\varepsilon)|^2=\tfrac{5}{14}|V_{\Gamma_{15}}(\varepsilon)|^2+\tfrac{9}{14}|V_{\Gamma_{25}}(\varepsilon)|^2 \ , \quad \text{(A13)}$$
$$|V_{\Gamma_7}(\varepsilon)|^2=\tfrac{3}{7}|V_{\Gamma_{25}}(\varepsilon)|^2 \ .$$

From these expressions and (A8)–(A10) it is immediately apparent that the Γ_6 level will be the most affected by the hybridization, followed by Γ_8 and Γ_7, which explains why the crystal-field splittings observed in the Yb pnictides are larger than expected from a straightforward extrapolation from pnictides of lighter rare earths, based on a point ion model.[3]

APPENDIX B: NUMERICAL DETAILS

All convolutions in the integral equations were performed by fast Fourier transform methods. A linear energy mesh with a step size 2×10^{-5} eV (4×10^{-5} eV) and

TABLE II. LCAO parameters (in Rydbergs) obtained from the fit of the band structure. We use the notation of Ref. 34; the parameters in brackets [e.g., $(ff\sigma)$] are in the two-center approximation. The rms deviation refers to 85 inequivalent points in the irreducible part of the Brillouin zone.

	YbN	YbP	YbAs
Metal			
$E_{s,s}(0,0,0)$	1.442 912 8	0.919 399 7	0.848 981 1
$E_{s,s}(1,1,0)$	−0.063 264 8	−0.003 909 6	−0.001 915 3
$E_{s,xy}(1,1,0)$	−0.008 942 3	−0.004 319 7	0.000 643 3
$E_{s,3z^2-r^2}(1,1,0)$	−0.039 730	−0.002 946 6	−0.019 509 2
$E_{xy,xy}(0,0,0)$	1.009 403	0.778 441 7	0.659 116 1
$E_{xy,xy}(1,1,0)$	−0.060 765 4	−.053 540 3	−0.037 468 9
$E_{xy,xy}(0,1,1)$	0.015 543 4	0.010 603 0	0.090 733
$E_{xy,xz}(0,1,1)$	−0.006 235 8	0.002 198 9	−0.007 468 5
$E_{xy,3z^2-r^2}(1,1,0)$	−0.035 581 2	−0.006 701 6	0.004 509 9
$E_{3z^2-r^2,3z^2-r^2}(0,0,0)$	1.170 023 2	0.887 523 9	0.877 004 9
$E_{3z^2-r^2,3z^2-r^2}(1,1,0)$	−0.007 324 5	−0.009 270 6	−0.005 737 7
$E_{x^2-y^2,x^2-y^2}(1,1,0)$	−0.011 376 8	0.001 803 2	−0.009 823 9
$E_{s,s}(2,0,0)$	0.022 089 9	−0.031 106 6	−0.020 902 1
$E_{s,3z^2-r^2}(0,0,2)$	0.038 719 2	0.037 676 6	0.021 275 8
$E_{xy,xy}(2,0,0)$	−0.013 849 0	−0.010 158 5	−0.006 007 5
$E_{xy,xy}(0,0,2)$	0.003 895 7	0.001 744 0	0.003 599 3
$E_{3z^2-r^2,3z^2-r^2}(2,0,0)$	−0.010 925 8	−0.049 401 1	−0.047 282 6
$E_{x^2-y^2,x^2-y^2}(0,0,2)$	−0.000 199 7	0.001 165 1	−0.002 971 5
$E_{z(x^2-y^2),z(x^2-y^2)}(0,0,0)$	0.502 799 3	0.387 813 5	0.164 416 4
$E_{xyz,xyz}(0,0,0)$	0.498 436 3	0.385 135 1	0.165 149 4
$E_{x(5x^2-3),x(5x^2-3)}(0,0,0)$	0.505 745 8	0.387 474 2	0.164 433 0
$(ff\sigma)_1$	0.001 103 9	−0.000 273 8	0.000 280 4
$(ff\pi)_1$	−0.000 497	−0.000 297 9	−0.000 566 9
$(ff\delta)_1$	0.000 653 2	0.000 149 9	0.000 082 3
$(ff\phi)_1$	−0.000 494 7	0.000 297	−0.000 048 8
$(sf\sigma)_1$	0.010 061 9	0.006 388 4	0.001 029 1

TABLE II. (*Continued*).

	YbN	YbP	YbAs
Metal			
$(df\sigma)_1$	−0.006 595 4	−0.000 446 6	−0.005 220 3
$(df\pi)_1$	0.003 267 0	0.000 911 6	0.000 617 0
$(df\delta)_1$	0.005 236 7	0.000 580 7	0.002 406 7
$(sf\sigma)_2$	−0.018 056 8	0.008 375 3	0.001 852 3
$(df\sigma)_2$	−0.007 251 7	0.005 004 6	−0.005 078 7
$(df\pi)_2$	0.002 455 2	−0.002 047 0	0.003 518 4
$(df\delta)_2$	−0.000 167 3	−0.002 009 2	−0.004 139 9
$(pf\sigma)_1$	0.013 196 5	0.004 647 7	0.000 981 8
$(pf\pi)_1$	0.006 821 5	−0.002 054 7	−0.003 878
$(pf\sigma)_2$	0.014 067 6	0.000 349 5	0.006 852 6
$(pf\pi)_2$	0.003 661 9	−0.001 391	0.006 726 2
$E_{x,x}(0,0,0)$	1.633 637 9	1.002 841 8	1.188 970 2
$E_{x,x}(1,0,0)$	−0.016 772 7	0.016 168 2	−0.022 248 9
$E_{x,x}(0,1,1)$	−0.077 749 3	−0.011 909 0	0.035 154 2
$E_{x,y}(1,1,0)$	0.053 743 7	−0.037 933 4	0.043 283 4
$E_{x,xy}(1,1,0)$	−0.052 708 8	−0.042 473 4	−0.025 171 9
$E_{x,xy}(0,1,1)$	0.024 582 3	0.011 601 7	0.012 091 9
$E_{z,3z^2-r^2}(0,1,1)$	0.011 696 9	0.001 297 6	0.032 235 1
$E_{z,x^2-y^2}(0,1,1)$	−0.021 252 8	−0.012 790 5	0.005 770 2
$E_{s,x}(1,1,0)$	−0.015 071 3	0.010 041 8	0.001 972 5
$E_{s,x}(2,0,0)$	0.054 983 1	0.020 703 8	0.020 588 3
$E_{x,x}(2,0,0)$	−0.034 001 4	0.016 637 4	0.066 607 2
$E_{y,y}(2,0,0)$	0.047 056 5	0.022 440 1	0.005 710 5
$E_{x,xy}(0,2,0)$	−0.023 566 3	−0.016 317 2	−0.005 113 3
$E_{z,3z^2-r^2}(0,0,2)$	−0.004 061 6	0.035 133 0	−0.038 816 3
Ligand			
$E_{s,s}(0,0,0)$	−0.201 346 8	−0.001 462 5	−0.109 686 1
$E_{s,s}(1,1,0)$	−0.014 235 8	−0.018 766 1	−0.022 748 0
$E_{x,x}(0,0,0)$	0.537 556 8	0.421 883 2	0.433 717 3
$E_{x,x}(1,1,0)$	0.004 135 7	0.002 645 4	0.023 426 9
$E_{x,x}(0,1,1)$	−0.001 806 8	0.004 606 5	0.000 636 2
$E_{x,y}(1,1,0)$	0.033 104 4	0.016 577 3	0.002 325 8
$E_{s,x}(1,1,0)$	−0.000 891 5	0.014 000	0.213 989
$E_{s,s}(2,0,0)$	−0.002 422 5	−0.003 183 5	−0.000 219 7
$E_{s,x}(2,0,0)$	0.004 210 5	−0.001 687 8	0.011 635 8
$E_{x,x}(2,0,0)$	0.005 811 6	0.028 582 1	0.003 332 8
$E_{y,y}(2,0,0)$	−0.000 011 3	−0.003 118 3	−0.005 021 8
Metal Ligand			
$E_{s,s}(1,0,0)$	0.057 739 8	−0.469 493	−0.005 466 8
$E_{s,x}(1,0,0)$	−0.010 404 3	0.082 033 8	0.100 073 0
$E_{3z^2-r^2,s}(0,0,1)$	0.139 194 9	0.132 607	0.134 131 6
$E_{xy,x}(0,1,0)$	0.052 429 3	0.057 580 5	0.079 943 6
$E_{3z^2-r^2,z}(0,0,1)$	0.165 419 2	0.087 468 2	0.102 032 7
$(fp\sigma)_1$	−0.016 413 6	−0.014 067 5	−0.008 974 6
$(fp\pi)_1$	0.019 577 0	0.013 969 3	0.010 897 1
$E_{x,x}(1,0,0)$	0.095 495 4	0.077 661 1	−0.053 464 3
$E_{y,y}(1,0,0)$	−0.021 226 5	−0.055 378 1	−0.043 597 3
$E_{x,s}(1,0,0)$	0.096 039 4	0.118 367 2	−0.110 009 7
$E_{xy,s}(1,1,1)$	0.004 503 2	0.001 331 1	−0.002 608 2
$E_{xy,x}(1,1,1)$	0.000 530	0.003 718 6	−0.000 751 1
$E_{x^2-y^2,x}(1,1,1)$	−0.001 102 1	0.000 349 9	0.
$E_{yz,x}(1,1,1)$	0.002 731 9	0.005 775 9	0.
$E_{s,s}(1,1,1)$	−0.016 085 3	−0.004 489 6	0.
$E_{s,x}(1,1,1)$	−0.002 551 3	0.005 217 7	0.
rms (mRy)	2.0	1.9	1.5

a periodically continued interval of 10.5 eV (21 eV) was used for the YbN and YbP (YbAs). As in Ref. 20, the calculations were started by a seed at high temperature and the converged values for $B(\varepsilon)$ and $A_{\Gamma_i}(\varepsilon)$ were used as input for the iterations at the next lower temperature. Due to the weak coupling of the Γ_7 level to the bands, calculations which included this level in the self-consistency cycle became unstable below 500 K, so that only the lowest and first excited level were considered explicitly. The two sum rules

$$\int B(\varepsilon)d\varepsilon=1 , \tag{B1}$$

$$2\int A_{\Gamma_6}(\varepsilon)d\varepsilon+4\int A_{\Gamma_8}(\varepsilon)d\varepsilon=6 , \tag{B2}$$

were satisfied to better than 0.5%, 1%, 0.4% for (B1) and 3%, 2.7%, 0.8% for (B2) at the lowest temperature considered for YbN, YnP, and YbAs, respectively, and to better than 10^{-3} above 30 K for all three compounds. In the sum rule on the occupied part of the f density of states

$$\int \rho^{<}(\omega)d\omega=n_f=2\int a_{\Gamma_6}(\omega)d\omega+4\int a_{\Gamma_8}(\omega)d\omega , \tag{B3}$$

the two expressions for n_f lead to values which, e.g., at 14.6 K differ by 3×10^{-4}, 6×10^{-3}, and 10^{-5} with, again, a better agreement at higher temperature.

APPENDIX C: INPUT BAND STRUCTURES AND LCAO PARAMETERS

For the sake of completeness, we show in Fig. 5 the self-consistent semirelativistic band structures of YbN, YbP, and YbAs. They are all characterized by a strong metal f-anion p hybridization and differ only in details. For the linear combination of atomic orbitals (LCAO) parametrization[34] we consider the rare-earth $4f$, $5d$, and $6s$ and the pnictide $3s$, $3p$ orbitals, with first- and second-neighbor metal-metal, ligand-ligand, and metal-liquid interactions, except for the direct f-f and the f-ligand coupling, where we take into account only nearest neighbors. We further make the two-center approximation for all integrals involving f orbitals. This leads to 72 independent parameters, listed in Table II.

[1]W. Stutius, Phys. Kondens. Mater. **10**, 152 (1969).

[2]H. R. Ott, F. Hullinger, and H. Rudigier, in *Valence Instabilities,* edited by P. Wachter and H. Boppart (North-Holland, Amsterdam, 1982), p. 511.

[3]R. J. Birgeneau *et al.*, Phys. Rev. B **8**, 5345 (1978).

[4]B. Hälg, A. Furrer, and F. Hulliger, Paul Scherrer Institute Report No. AF-SSP-127, 1984 (unpublished).

[5]A. Furrer (private communication).

[6]H. R. Ott, H. Rudigier, and F. Hulliger, Solid State Commun. **55**, 113 (1985).

[7]P. Bonville *et al.*, J. Magn. Magn. Mater. **63 & 64**, 626 (1987).

[8]P. Bonville *et al.*, Hyperfine Interact. **40**, 381 (1988).

[9]A. M. Tsvelick and P. B. Wiegmann, J. Phys. C **15**, 1707 (1982).

[10]J. W. Rasul, in *Valence Instabilities,* edited by P. Wachter and H. Boppart (North-Holland, Amsterdam, 1982), p. 49.

[11]N. Andrei, K. Furuya, and J. H. Lowenstein, Rev. Mod. Phys. **55**, 331 (1983).

[12]P. Schlottmann, Z. Phys. B **49**, 109 (1982).

[13]V. T. Rajan, Phys. Rev. Lett. **51**, 308 (1983).

[14]P. Schlottmann, Z. Phys. B **56**, 127 (1984).

[15]A. C. Hewson and J. W. Rasul, J. Phys. C **16**, 6799 (1983).

[16]P. Schlottmann, Z. Phys. B **55**, 293 (1984); Phys. Rev. B **30**, 1454 (1984).

[17]N. Kawakami and K. Okiji, J. Phys. Soc. Jpn. **54**, 685 (1985).

[18]H. U. Desgranges and J. W. Rasul, Phys. Rev. B **32**, 6100 (1985); Phys. Rev. B **36**, 328 (1987).

[19]For a quartet and a doublet separated by a splitting A, Ref. 17 gives $T_{\text{eff}}/T_0=0.234(T_0/A)^2$; Ref. 18 considers the case of two doublets separated by A: $T_{\text{eff}}/T_0=0.300/(T_0/A)$, and three equidistant doublets: $T_{\text{eff}}/T_0=0.029(T_0/A)^2$.

[20]N. E. Bickers, D. L. Cox, and J. W. Wilkins, Phys. Rev. B **36**, 2036 (1987); Phys. Rev. Lett. **54**, 230 (1985).

[21]F. C. Zhang and T. K. Lee, Phys. Rev. B **30**, 1556 (1984).

[22]P. Coleman, Phys. Rev. B **29**, 3035 (1984).

[23]Y. Kuramoto, Z. Phys. B **53**, 37 (1983).

[24]From Ref. 70 in N. E. Bickers, D. L. Cox, and J. W. Wilkins, Phys. Rev. B **36**, 2036 (1987), the self-consistent approach should be reliable down to $0.1T_{\text{eff}}$.

[25]R. Monnier, L. Degiorgi, and D. D. Koelling, Phys. Rev. Lett. **56**, 2744 (1985).

[26]These will be renormalized through the mixing term in the Hamiltonian. The particularly spectacular case of the Ce pnictides (Ref. 3) has been treated by P. Thayambali and B. R. Cooper, Rev. B **30**, 2931 (1984), and J. M. Wills and B. R. Cooper, Phys. Rev. B **36**, 3809 (1987).

[27]E. Müller-Hartmann, Z. Phys. B **57**, 281 (1984).

[28]The error on the partition function and *a fortiori* on the specific heat is extremely sensitive to the choice of ε_0, which has to be within $\approx k_B T$ of the NCA ground-state energy E_0 if accurate results are to be obtained. Note, however, that the factor $e^{\beta\varepsilon_0}$ cancels on both sides of Eqs. (8a) and (8b), which can therefore be solved for $\varepsilon_0=0$ with the appropriate normalization.

[29]T. Greber *et al.*, J. Phys. (Paris) C **9**, 943 (1987).

[30]O. Gunnarsson and K. Schoenhammer, Phys. Rev. B **28**, 4315 (1983).

[31]For comparison with Rajan's (Ref. 13) Bethe ansatz results for an isolated doublet the spin susceptibility is normalized to its zero-temperature value obtained from a cubic fit to the inverse of the calculated $\chi(T)$.

[32]Y. Kuramoto and H. Kojima, Z. Phys. B **57**, 95 (1984).

[33]A. Okiji and N. Kawakami, J. Magn. Magn. Mater. **54-57**, 327 (1986).

[34]J. C. Slater and G. F. Koster, Phys. Rev. **94**, 1498 (1954); K. Takegahara, Y. Aoki, and A. Yanase, J. Phys. C **13**, 583 (1980).